

# Journal of Biomedical Optics

[SPIEDigitalLibrary.org/jbo](http://SPIEDigitalLibrary.org/jbo)

## **Targeting tumor hypoxia with 2-nitroimidazole-indocyanine green dye conjugates**

Yan Xu  
Saeid Zanganeh  
Innus Mohammad  
Andres Aguirre  
Tianheng Wang  
Yi Yang  
Liisa Kuhn  
Michael B. Smith  
Quing Zhu

# Targeting tumor hypoxia with 2-nitroimidazole-indocyanine green dye conjugates

Yan Xu,<sup>a\*</sup> Saeid Zanganeh,<sup>a\*</sup> Innus Mohammad,<sup>b</sup> Andres Aguirre,<sup>a</sup> Tianheng Wang,<sup>a</sup> Yi Yang,<sup>a</sup> Liisa Kuhn,<sup>c</sup> Michael B. Smith,<sup>b</sup> and Quing Zhu<sup>a</sup>

<sup>a</sup>University of Connecticut, Electrical and Computer Engineering and Biomedical Engineering Departments, Storrs, Connecticut 06269

<sup>b</sup>University of Connecticut, Chemistry Department, Storrs, Connecticut 06269

<sup>c</sup>University of Connecticut Health Center, Department of Reconstructive Sciences, Farmington, Connecticut 06030

**Abstract.** Tumor hypoxia is a major indicator of treatment resistance to chemotherapeutic drugs, and fluorescence optical tomography has tremendous potential to provide clinically useful, functional information by identifying tumor hypoxia. The synthesis of a 2-nitroimidazole-indocyanine green conjugate using a piperazine linker (piperazine-2-nitroimidazole-ICG) capable of robust fluorescent imaging of tumor hypoxia is described. *In vivo* mouse tumor imaging studies were completed and demonstrate an improved imaging capability of the new dye relative to an earlier version of the dye that was synthesized with an ethanolamine linker (ethanolamine-2-nitroimidazole-ICG). Mouse tumors located at imaging depths of 1.5 and 2.0 cm in a turbid medium were imaged at various time points after intravenous injection of the dyes. On average, the reconstructed maximum fluorescence concentration of the tumors injected with piperazine-2-nitroimidazole-ICG was twofold higher than that injected with ethanolamine-2-nitroimidazole-ICG within 3 h postinjection period and 1.6 to 1.7 times higher beyond 3 h postinjection. The untargeted *bis*-carboxylic acid ICG completely washed out after 3 h postinjection. Thus, the optimal window to assess tumor hypoxia is beyond 3 h postinjection. These findings were supported with fluorescence images of histological sections of tumor samples and an immunohistochemistry technique for identifying tumor hypoxia. © 2013 Society of Photo-Optical Instrumentation Engineers (SPIE) [DOI: 10.1117/1.JBO.18.6.066009]

Keywords: tumor hypoxia; fluorescence tomography; indocyanine green; 2-nitroimidazole.

Paper 130211PR received Apr. 7, 2013; revised manuscript received Apr. 23, 2013; accepted for publication May 2, 2013; published online Jun. 13, 2013.

## 1 Introduction

Tumor hypoxia is a major indicator of cancer resistance to chemotherapeutic drugs.<sup>1</sup> Noninvasive imaging of tumor hypoxia has important clinical utility in predicting cancer treatment outcomes and offers the possibility of tailored chemotherapeutic regimens that may enhance the probability of complete tumor remission. Nitroimidazoles are a well-studied class of molecular probes that target tumor hypoxia by nucleophilic covalent binding to proteins in environments of low pO<sub>2</sub> (<1.5% O<sub>2</sub>).<sup>2-4</sup> Among all the imidazole compounds, 2-nitroimidazoles have higher electron affinities and are the most commonly used hypoxia markers when labeled with positron emission tomography (PET) radionuclides.<sup>5,6</sup> Problems associated with PET radionuclides include low resolution, high background counts, and the use of radioactive tracers. In addition, PET systems are expensive for routine clinical use in longitudinal imaging assessments over the course of chemotherapy. Thus there is a need for the development of safer, alternative techniques for imaging tumor hypoxia and improving cancer patient outcomes.

The development of fluorescence diffused optical tomography (FDOT) techniques in the near-infrared (NIR) spectrum is expected to have significant impact on future personalized oncology treatments owing to the very low tissue autofluorescence and high tissue penetration depth in the NIR spectrum window.<sup>7-10</sup> Cancer NIR molecular imaging relies greatly on

the development of stable, highly specific and sensitive molecular probes.<sup>11-16</sup> Organic dyes such as indocyanine green have been used as nontargeted agents for optical imaging of cancer and have been used clinically for many years.<sup>17,18</sup> By combining these two molecules, we have developed a novel nitroimidazole indocyanine dye conjugate (2-nitroimidazole-ICG dye conjugate) for tumor-targeted hypoxia fluorescence tomography.<sup>19</sup> The *bis*-carboxylic acid ICG derivative was synthesized and used in our studies (hereafter cited as ICG). The 2-nitroimidazole-ICG dye conjugate hypoxia probe has been evaluated *in vitro* using tumor cells and *in vivo* using a mouse tumor model to confirm the capability of the novel probe to identify hypoxic environments.<sup>20</sup> *In vivo* tumor targeting studies in mice showed that the fluorescence signals measured at the tumor site were twice those at the normal site after 150 min postinjection of the hypoxia probe. The fluorescence signals measured after injection of ICG alone were the same at the tumor and normal sites, indicating a lack of tumor targeting and further proving the importance of the 2-nitroimidazole. *In vivo* fluorescence tomography images of mice injected with the hypoxia probe showed that the probe remained for more than 5 to 7 h in the tumors. However, the images of mice injected with ICG confirmed that the unbound dye washed out in less than 3 h. These findings were supported with fluorescence images of histological sections of tumor samples using a commercial infrared scanner and immunohistochemistry (IHC) to independently identify tumor hypoxia. In this paper, we report on the synthesis of a second-generation 2-nitroimidazole-ICG conjugate using a more stable piperazine linker to conjugate the 2-nitroimidazole

\*The first two authors contributed equally to this study.

Address all correspondence to: Quing Zhu, University of Connecticut, Electrical and Computer Engineering and Biomedical Engineering Departments, Storrs, Connecticut 06269. Tel: +860-486-5523; Fax: +860-486-2447; E-mail: [zhu@enr.uconn.edu](mailto:zhu@enr.uconn.edu)

and *bis*-carboxylic acid ICG (piperazine-2-nitroimidazole-ICG) moieties. We have compared the performance of the second-generation hypoxia probe with the earlier version and systematically evaluated its sensitivity in an *in vivo* murine tumor model with tumors located at depths of 1.5 and 2 cm inside turbid medium emulating biological tissue. These studies demonstrate that the new piperazine linker significantly improved *in vivo* fluorescence signal strength relative to that of the first-generation dye synthesized with an ethanolamine linker (ethanolamine-2-nitroimidazole-ICG).

## 2 Materials and Methods

### 2.1 Synthesis of 2-nitro-ICG Dye Conjugates

The details of the synthetic procedures used to prepare the dye conjugates, as well as the photophysical and chemical properties and the optical stability of the first-generation dye, ethanolamine-2-nitroimidazole-ICG (compound 4), and related compounds have been previously described.<sup>19</sup> Briefly, as shown in Fig. 1, methyl 2-nitroimidazoleacetate (compound 1) was coupled to ethanolamine to yield compound 2. Subsequent dehydrative coupling with indocyanine dicarboxylic acid (compound 3) yielded compound 4. This work describes the preparation of compound 2, the synthesis of compound 3, and coupling procedures to prepare compound 4. Both the *bis*-carboxylic acid ICG derivative and the 2-nitroimidazole-ICG have an absorption peak around 755 to 760 nm, and a fluorescent emission peak at 778 nm, with a quantum yield of 0.0728, which is six times higher than that of commercially available ICG purchased from Sigma-Aldrich, St. Louis. For the studies described in this manuscript, the synthesis was modified to change the ethanolamine linker to a piperazine linker. This modification of the original sequence yielded compound 9 (see Fig. 2). The goal of this modification was to produce a dye conjugate that was more robust *in vivo*, with two amide linkages rather than an

amide and an ester. As shown in Fig. 2, the synthesis of compound 9 began by the preparation of the Boc protected piperazine in 35% yield using a literature procedure.<sup>21</sup> Subsequent treatment with bromoacetyl bromide gave compound 6 in 81% yield, and subsequent coupling to 2-nitroimidazole<sup>22</sup> gave compound 7 in 94% yield. Deprotection of Boc group with trifluoroacetic acid gave trifluoroacetyl salt (compound 8) in 86% yield, which was coupled to ICG-*bis*(carboxylic acid) (compound 3) by the same coupling procedure used to prepare compound 4 (Ref. 23), giving 2-nitropiperazine ICG dye conjugate (compound 9) in 21% yield based on compound 3.

The piperazine-2-nitroimidazole-ICG, ethanolamine-2-nitroimidazole-ICG, and *bis*-carboxylic acid ICG were spectrally characterized by using a UV-Vis spectrophotometer and a fluorescence spectrophotometer (Varian Analytical Instruments, Walnut Creek, California). The wavelength range of both spectrophotometers is 250 to 1100 nm. The relative quantum yield of each dye was calculated as  $\Phi_x = \Phi_{ST} \text{Grad}_x / \text{Grad}_{ST} \eta_x^2 / \eta_{ST}^2$ ,<sup>24,25</sup> where Grad was the gradient or slope from the plot of the integrated fluorescence intensity versus absorbance measured at different concentrations, x is any unknown dye, ST is the standard dye, and  $\eta$  is the refractive index of the solvent. ICG from Sigma-Aldrich of quantum yield 0.012 (Ref. 26) was used as a standard. The excitation wavelength of 730 nm was used for all quantum yield measurements. Figure 3 shows the measured absorption and emission spectra of four dyes. Since the standard and unknown dyes were measured in the same solvent, the refractive index effects were canceled. All the dyes were measured at very low concentration to avoid the self-quenching effects. The extinction coefficient of each dye was measured using a certain amount of dye powder weighed and diluted in a known volume of sucrose solution to maintain a fixed concentration ( $\mu\text{M}/l$ ). The sample path length was 10 mm. The absorbance was measured in the UV-Vis spectrophotometer, and Beer-Lambert's law was used to calculate the extinction coefficient from the peak absorbance of the dye with a

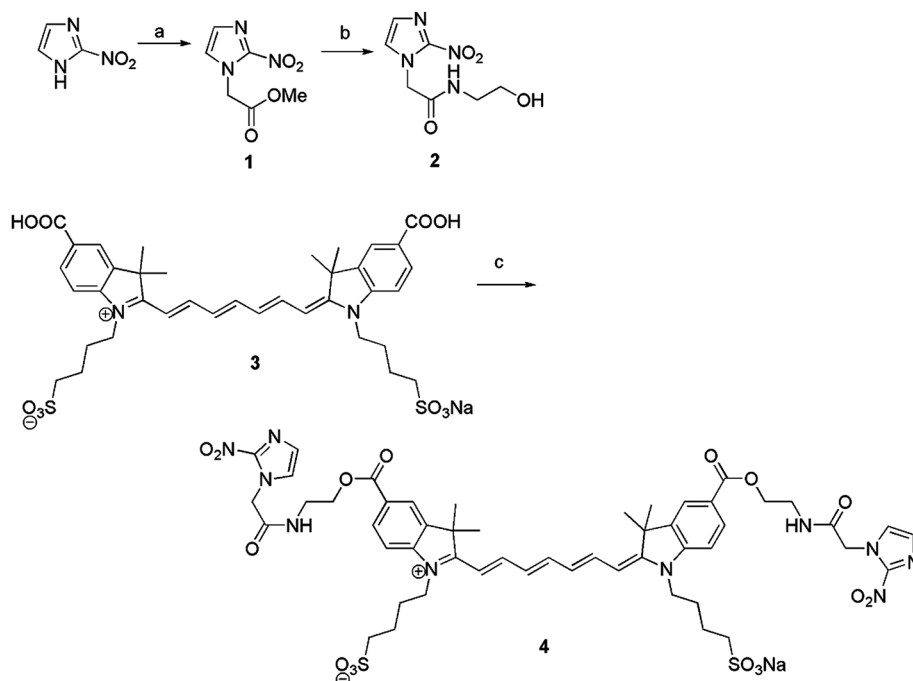


Fig. 1 Synthesis Scheme 1.

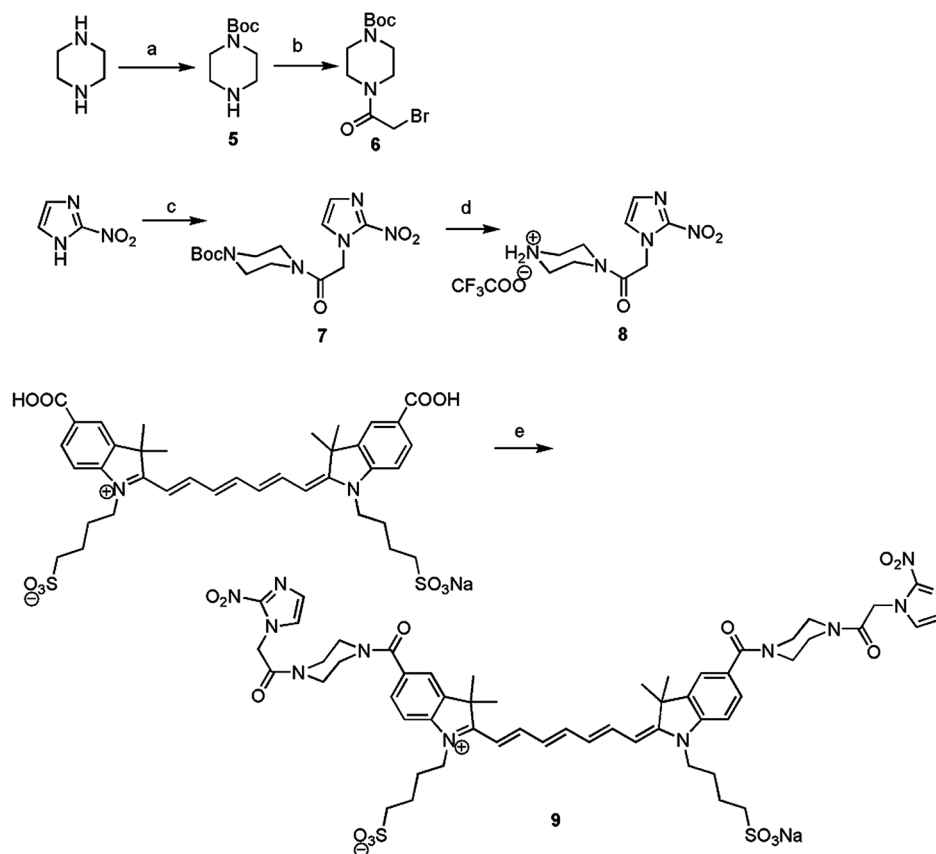


Fig. 2 Synthesis Scheme 2.

known concentration. The optical properties of all the compounds are given in Table 1.

## 2.2 Murine Tumor Model

*In vivo* tumor imaging experiments were performed using a murine tumor model (4T1 Luc mouse mammary carcinoma cells grown in BALB/c mice). The animal protocol was approved by the Institutional Animal Care and Use Committee of University of Connecticut. 4T1 Luc cells were cultured at 37°C with 5%

CO<sub>2</sub> in Roswell Park Memorial Institute 1640 medium (Gibco, USA), supplemented with 10% fetal bovine serum, 50 U/mL penicillin/streptomycin, 2 mM l-glutamine, and 1 mM pyruvate. The 4T1 Luc cells were passed three times at 70 to 80% confluence in a T75 flask (BD Biosciences, Bedford, Massachusetts) prior to injection, and 1 × 10<sup>5</sup> cells were injected into the lower right mammary fat-pad of seven-week-old BALB/c female mice. The experiments were performed when the tumor sizes reached approximately 7 to 9 mm in diameter, two to three weeks postinoculation.

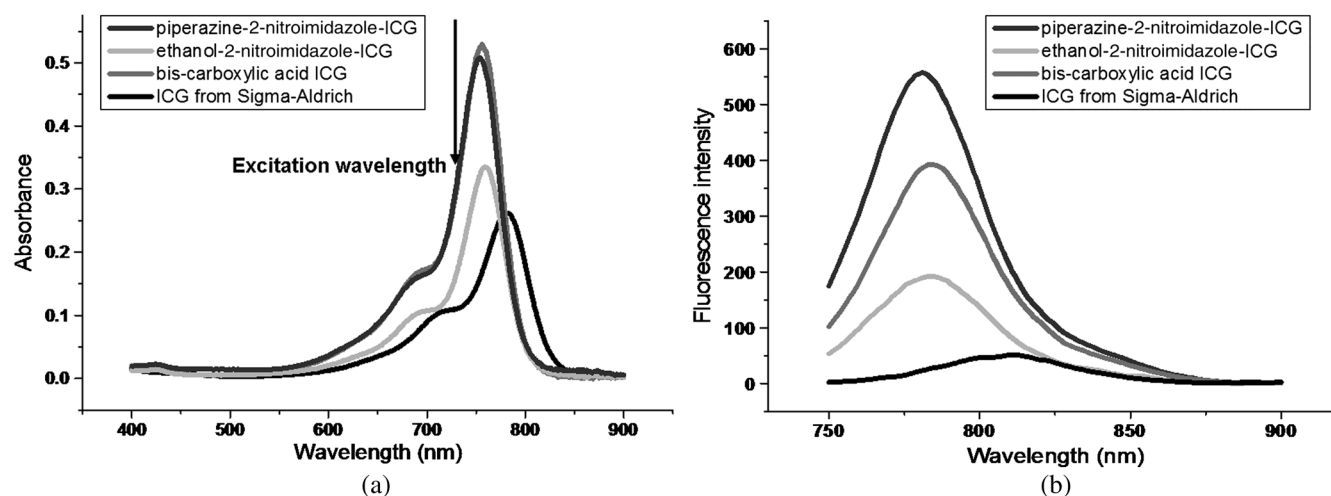


Fig. 3 (a) Spectra of absorbance of piperazine-2-nitroimidazole-ICG, ethanol-2-nitroimidazole-ICG, bis-carboxylic acid ICG, and ICG from Sigma-Aldrich. (b) Corresponding fluorescence emission intensity versus wavelength measured at the excitation wavelength of 730 nm. All the samples were in 2.35 μM concentration.

**Table 1** The optical properties of ICG from Sigma-Aldrich, bis-carboxylic acid ICG, ethanolamine-2-nitroimidazole-ICG, and piperazine-2-nitroimidazole-ICG.

Compound	$\lambda_{\text{abs}}^{\text{max}}$ (nm)	$\lambda_{\text{ems}}^{\text{max}}$ (nm)	Extinction coefficient $\epsilon$ ( $\text{M}^{-1} \text{cm}^{-1}$ )	Quantum yield ( $\Phi$ )
ICG from Sigma-Aldrich	780	807	115000	0.012
bis-carboxylic acid ICG	755	790	220920	0.0728
ethanolamine-2-nitroimidazole-ICG	760	790	159141	0.0420
piperazine-2-nitroimidazole-ICG	760	790	229543	0.0825

Note:  $\lambda_{\text{abs}}^{\text{max}}$  is the wavelength measured at the maximum absorption spectrum, and  $\lambda_{\text{ems}}^{\text{max}}$  is the wavelength measured at the maximum emission spectrum.

Because tumor hypoxia environment depends largely on tumor size,<sup>27</sup> the hypoxia conditions for different groups of mice injected with different dyes should be statistically similar.

### 2.3 FDOT System and Tumor Imaging

The *in vivo* experiments were performed using a frequency domain fluorescence imaging system, which consisted of 14 parallel detectors and 4 laser diodes of 690, 780, 808, and 830 nm. Each laser diode was sequentially switched to nine positions on a hand-held probe (see Fig. 4). The excitation wavelength used in this study was 690 nm. The 14-channel parallel detection system has two modes: fluorescence mode and absorption mode. The two modes can be easily switched by moving a mechanical handle. A stopper was designed in the system to ensure a precise optical collimation when switching between these two modes. Note that in the fluorescence mode, a bandpass filter was placed in the light path to remove the excitation and stray light; in the absorption mode, the bandpass filter was moved out of the light path. Fourteen photomultiplier tubes were used as detectors, and the received signals were amplified by preamplifiers, mixed by mixers, low pass filtered, and further amplified before analog to digital converters. Two National Instrument data acquisition cards of eight channels each were used to acquire FDOT data.

One group of mice was injected intravenously through retro-orbital injections with 100  $\mu\text{l}$  of ICG ( $n = 4$  mice) at 50 and 25  $\mu\text{M}$  concentrations, respectively, as control, and the second group was injected with 100  $\mu\text{l}$  of piperazine-2-nitroimidazole-ICG at 50 ( $n = 2$ ), 25 ( $n = 3$ ), and 15  $\mu\text{M}$  ( $n = 3$ ) concentrations, respectively. The last group was injected with 100  $\mu\text{l}$  ethanolamine-2-nitroimidazole-ICG at 50 ( $n = 2$ ) and 25  $\mu\text{M}$  ( $n = 2$ ) concentrations to compare with results obtained from piperazine-2-nitroimidazole-ICG.

Each mouse, anesthetized with inhalation of 1.5% isoflurane, was mounted on a thin glass plate facing the probe with the lower mammary pads submerged in the Intralipid solution, with a typical soft tissue absorption coefficient  $\mu_a = 0.02$  to  $0.03 \text{ cm}^{-1}$  and reduced scattering coefficient  $\mu_s' = 6$  to  $8 \text{ cm}^{-1}$ . The tumor was imaged for up to 1 min postinjection and again at 15 min, 30 min, 1, 2, 3, 5, and 7 h. The center of the probe was aligned to the center of the tumor and the separation between the tumor center and the probe surface was defined as the imaging depth for fluorescence images. Several imaging data sets were collected to compare the *in vivo* imaging sensitivity of two hypoxia dye conjugates versus ICG at different concentrations and tumors located at different depths.

### 2.4 Fluorescence Imaging Reconstruction

To reconstruct fluorescence images, a normalized Born approximation has been widely used.<sup>28,29</sup> This normalization eliminates unknown system parameters, i.e., source strengths, gains of different detectors, background optical properties of the tissue, coupling efficiency to the tissue, etc. This normalized Born ratio was adopted in our early study<sup>16</sup> as well as this study and is given as

$$\phi^{nB}(r_s, r_d) = \frac{\phi_{fl}(r_s, r_d)}{\phi_{exc}(r_s, r_d)},$$

where  $\phi^{nB}$  is the normalized Born ratio,  $\phi_{fl}$  is the fluorescence measurement after subtraction of the system noise measurement without any fluorophores or targets in the background medium, and  $\phi_{exc}$  is the excitation measurement at 690 nm. For inversion, a dual-zone mesh method was used to reconstruct the fluorophore concentrations at the target depth and the background regions described previously.<sup>16</sup>

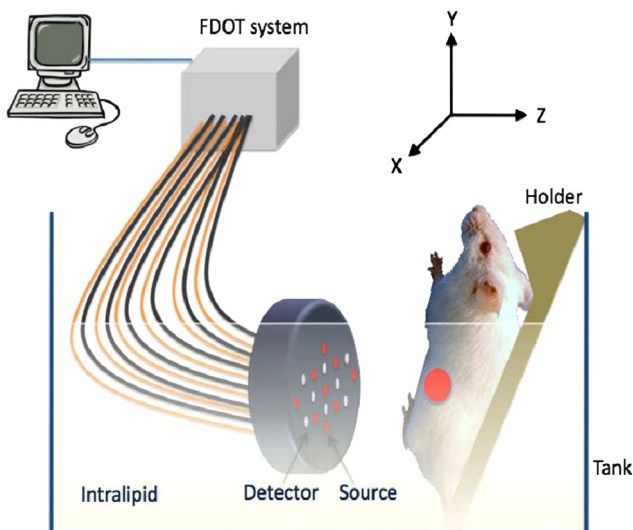


**Fig. 4** *In vivo* fluorescence imaging set-up.

## 2.5 Immunohistochemistry

Hypoxyprobe<sup>TM</sup>-1 plus kit from HPI Inc., Burlington, Massachusetts, was used to visualize the hypoxia tumor areas using an IHC technique. Based on the protocol recommended by the company, 45 min before the animal was euthanized, 1.5 mg of Hypoxyprobe<sup>TM</sup>-1 plus kit diluted in 100  $\mu$ l of 0.9% saline solution was injected intravenously. Immediately after the animal was euthanized, the tumor was harvested. The tumor specimens were collected and directly frozen in liquid nitrogen until cryosectioned into 10  $\mu$ m sections. The prepared sections were stored at  $-80^{\circ}\text{C}$  before staining. After thawing, the sections were fixed in cold acetone for 10 min. Sections were rinsed and incubated overnight at  $4^{\circ}\text{C}$  with rabbit anti-pimonidazol antisera PA2627 diluted 1:20 in phosphate buffered saline (PBS) containing 0.1% bovine serum albumin and 0.1% Tween 20. The sections were then incubated for 60 min with fluorescein isothiocyanate-conjugated goat anti-rabbit antibody. Between all steps of the staining procedure, the sections were rinsed three times with PBS for 5 min each.

Digital images of the stained sections were obtained using an optical microscope at  $40\times$  and  $400\times$  magnifications. The percentage of hypoxic areas was analyzed using the Image *J* program (National Institutes of Health, Bethesda, Maryland). For this purpose, obtained digital images were transferred to the Image *J* software and all color images were converted to grayscale. Automated routine was used to threshold the images (same threshold for all mice images). The polygon selection tool was used to delineate the boundaries of the hypoxic areas. The percentage of hypoxia was defined as the number of pixels above the threshold in hypoxic areas over the total number of pixels of the total area analyzed.

## 2.6 Fluorescence Images of Tumor Samples

To validate the *in vivo* FDOT imaging results, excised tumor samples were imaged using a commercially available Odyssey Imaging system (Li-COR Biosciences, Nebraska). Using this system, 10  $\mu$ m tumor sample sections were dried and imaged at the highest scan resolution available (i.e., 21  $\mu$ m). The excitation channel selected was 785 nm and emission was 820 nm with a bandwidth of 40 to 50 nm. The images were obtained using the analysis software provided by the company. The mean pixel value of the images including the entire tumor sample area was measured using Image *J*.<sup>30</sup>

## 2.7 Experimental Details on the Synthesis of the Dye Conjugates

All chemicals were used as received from Aldrich or Acros. All glassware was flame-dried under vacuum, and all reactions in organic solvents were performed under a nitrogen atmosphere, unless otherwise noted. All solvents were dried according to standard procedures. Tetrahydrofuran was distilled from sodium benzophenone ketyl, methylene chloride was distilled from calcium hydride, and dimethylformamide was vacuum distilled from calcium hydride. Thin-layer chromatography (TLC) was done on Sorbent Technologies aluminum-backed thin-layer chromatography plates with fluorescent indicator and 0.2 mm silica gel layer thickness, and either *p*-anisaldehyde or phosphomolybdic acid were used as developing agents. Column chromatography was done using 60  $\text{\AA}$  porosity, 32 to 63  $\mu$ m silica gel. Both  $^1\text{H}$  and  $^{13}\text{C}$  NMR spectra were collected on a

Brüker Avance 300 (300.13 MHz  $^1\text{H}$ , 75.48 MHz  $^{13}\text{C}$ ), Brüker DRX-400 (400.144 MHz  $^1\text{H}$ , 100.65 MHz  $^{13}\text{C}$ ), or a Brüker Avance 500 (500.13 MHz  $^1\text{H}$ , 125.65 MHz  $^{13}\text{C}$ ). Chemical shifts are given in ppm ( $\delta$ ), downfield from TMS in the following format: chemical shift, multiplicity (*s* = singlet, *d* = doublet, *t* = triplet, *q* = quartet, *m* = multiplet), coupling constant in Hz, and integration. Mass spectroscopy data were collected on an HP 5870B GC/MSD mass spectrometer with an HP-1 column, and high-resolution mass spectrometry was done on a Micromass VB-QTOF tandem mass spectrometer. IR spectra were taken on FT/IR-410/C031560585 JASCO and Nexus 670 FT-IR E.S.P under neat conditions unless otherwise stated. Melting points were taken on a Uni-melt capillary melting point apparatus and Digimel MPA160 and recorded to a maximum of  $270^{\circ}\text{C}$ . For products described as waxy solid, melting points could not be obtained.

### 2.7.1 *Tert*-butyl piperazine-1-carboxylate (compound 5)

Di-*tert*-butyl dicarbonate (2.54 g, 11.6 mmol) in  $\text{CH}_2\text{Cl}_2$  (30 mL) was added to a stirring solution of piperazine (2 g, 23.2 mmol) in  $\text{CH}_2\text{Cl}_2$  (60 mL) at room temperature and stirred for 16 h. Solvents were removed under reduced pressure and the residue dissolved in water (50 mL). The aqueous solution was extracted with methylene chloride ( $4 \times 60$  mL) and all the organic extractions were combined, dried over anhydrous magnesium sulfate, and concentrated to get *tert*-butyl piperazine-1-carboxylate (compound 5) as a colorless oil (1.5 g, 8.05 mmol, 34.7% based on piperazine);  $^1\text{H}$  NMR (400 MHz,  $\text{CDCl}_3$ ):  $\delta$ 3.37 (*t*, *J* = 4 Hz, 2 H), 2.79 (*t*, *J* = 4 Hz, 2 H), 1.72 (bs, 1 H), 1.44 (s, 9 H) ppm;  $^{13}\text{C}$  NMR (100.6 Hz,  $\text{CDCl}_3$ ):  $\delta$ 154.3, 79.8, 45.6, 44.5, 28.8 ppm.

### 2.7.2 *Tert*-butyl 4-(2-bromoacetyl) piperazine-1-carboxylate (compound 6)

Triethylamine (0.5 mL, 3.5 mmol) was added to a stirring solution of *tert*-butyl piperazine-1-carboxylate (compound 5) (0.60 g, 3.22 mmol) in dry dichloromethane (25 mL) at  $0^{\circ}\text{C}$  and stirred for 15 min. Bromoacetyl bromide (0.3 mL, 3.5 mmol) was added dropwise at  $0^{\circ}\text{C}$ , and the resulting mixture was stirred at room temperature overnight. Reaction progress was monitored by TLC, and after disappearance of the starting material, the mixture was concentrated and purified via column chromatography (petroleum ether: ethyl acetate 15 to 20%) to give *tert*-butyl 4-(2-bromoacetyl) piperazine-1-carboxylate (compound 6) as a white solid (0.8 g, 2.6 mmol, 80.7%): Mp:  $95$  to  $97^{\circ}\text{C}$ .  $^1\text{H}$  NMR (400 MHz,  $\text{CDCl}_3$ ):  $\delta$ 3.85-3.84 (*d*, *J* = 4 Hz, 2 H), 3.59-3.57 (*t*, *J* = 6 Hz, 2 H), 3.49-3.48 (*m*, 4 H), 3.43-3.40 (*m*, 2 H), 1.45 (s, 9 H);  $^{13}\text{C}$  NMR (100 MHz,  $\text{CDCl}_3$ ):  $\delta$ 165.7, 154.7, 80.7, 46.8, 42.2, 28.6, 25.8; HRMS Calcd  $\text{C}_{11}\text{H}_{19}\text{BrN}_2\text{O}_3$  307.0657, found 307.0652.

### 2.7.3 *Tert*-butyl 4-(2-(2-nitro-1 *H*-imidazol-1-yl)acetyl) piperazine-1-carboxylate (compound 7)

Sodium hydride (0.025 g, 1.06 mmol) was added to a stirring solution of commercially available 2-nitroimidazole (0.1 g, 0.88 mmol) in dry DMF (1 mL), under an  $\text{N}_2$  atmosphere at  $0^{\circ}\text{C}$ , and stirred at  $0^{\circ}\text{C}$  for 30 min. At this time, *tert*-butyl 4-(2-bromoacetyl) piperazine-1-carboxylate (compound 6, 0.272 g, 0.88 mmol) was added slowly and the reaction mixture was stirred at room temperature overnight. The DMF was

evaporated and water (5 mL) was added to give a white precipitate, which was filtered and dried *in vacuo* to give an amorphous white powder, identified as *tert*-butyl 4-(2-(2-nitro-1H-imidazol-1-yl)acetyl)piperazine-1-carboxylate (compound 7, 0.28 g, 0.83 mmol, 94.3%). <sup>1</sup>H NMR (400 MHz, CDCl<sub>3</sub>): δ7.19 – 7.18 (*d*, *J* = 4 Hz, 1 H), 7.05 (*s*, 1 H), 5.21 (*s*, 2 H), 3.60 – 3.57 (*m*, 4 H), 3.50 (*m*, 2 H), 3.46 – 3.45 (*m*, 2 H), 1.46 (*s*, 9 H); <sup>13</sup>C NMR (100 MHz, CDCl<sub>3</sub>): δ163.4, 154.6, 148.2, 137.4, 121.5, 81.0, 49.0, 45.0, 42.5, 28.6; HRMS Calcd C<sub>14</sub>H<sub>22</sub>N<sub>5</sub>O<sub>5</sub> 340.1621, found 340.1608.

#### 2.7.4 2-(2-nitro-1 H-imidazol-1-yl)-1-(piperazin-1-yl)ethanone, TFA salt (compound 8)

Dropwise addition of trifluoroacetic acid (1 mL) to a stirred solution of *tert*-butyl 4-(2-(2-nitro-1 H-imidazol-1-yl)acetyl)piperazine-1-carboxylate (compound 7, 0.28 g, 0.83 mmol) in dry chloroform (10 mL) was followed by stirring overnight at room temperature. The reaction mixture was concentrated and triturated with ethyl acetate to give 2-(2-nitro-1H-imidazol-1-yl)-1-(piperazin-1-yl)ethanone, TFA (compound 8) as a white solid, which was filtered and dried *in vacuo* (0.25 g, 0.71 mmol, 85.5%); Mp: 95 to 96°C, and used without further purification. <sup>1</sup>H NMR (400 MHz, D<sub>2</sub>O) δ7.58 (*s*, 1 H), 7.40 (*s*, 1 H), 5.68 (*s*, 2 H), 4.08 (*t*, *J* = 4 Hz, 2 H), 4.03 – 4.00 (*m*, 2 H), 3.59 (*t*, *J* = 4 Hz, 2 H), 3.50-3.47 (*m*, 2 H); <sup>13</sup>C NMR (100 MHz, D<sub>2</sub>O) δ166.9, 163.3, 162.9, 162.6, 149.0, 129.2, 128.4, 121.0, 118.1, 115.2, 112.2, 51.3, 43.3, 42.2, 39.6; HRMS Calcd C<sub>10</sub>H<sub>14</sub>F<sub>3</sub>N<sub>5</sub>O<sub>5</sub> 240.1096, found 240.1149.

#### 2.7.5 Monosodium(II) mono(4-((Z)-2-((2E,4E,6E)-7-(3,3-dimethyl-5-(4-(2-(2-nitro-1 H-imidazol-1-yl)acetyl)piperazine-1-carbonyl)-1-(4-sulfonatobutyl)-3 H-indolium-2-yl)hepta-2,4,6-trienylidene)-3,3-dimethyl-5-(4-(2-(2-nitro-1 H-imidazol-1-yl)acetyl)piperazine-1-carbonyl)indolin-1-yl)butane-1-sulfonate) (compound 9)

A stirred solution of ICG *bis* (carboxylic acid) (**3**, 0.2 g, 0.26 mmol) in dry DMF (2 mL) at 0°C was treated with benzotriazol-1-yl-oxytripyrrolidinophosphonium hexafluorophosphate (0.30 g, 0.57 mmol), 1-hydroxybenzotriazole (0.08 g, 0.57 mmol), and diisopropylethylamine (220 μL, 0.57 mmol) in that order, and stirred at 0°C for 15 min. At this time, 2-(2-nitro-1H-imidazol-1-yl)-1-(piperazin-1-yl)ethanone, TFA salt (**8**, 0.204 g, 0.57 mmol) was added and the resulting mixture stirred at room temperature for 48 h. The DMF was evaporated and the resulting solid was purified using C18 reverse phase column chromatography to yield compound 9 as an amorphous green solid (0.065 g, 0.054 mmol, 20.7% based on **3**). <sup>1</sup>H NMR (400 MHz, D<sub>2</sub>O): δ7.84 (*t*, *J* = 12 Hz, 2 H), 7.57 (*s*, 2 H), 7.45 (*bs*, 5 H), 7.35–7.33 (*m*, 2 H), 7.27 (*s*, 2 H), 6.57 (*t*, *J* = 12 Hz, 2 H), 6.29 (*d*, *J* = 12 Hz, 2 H), 5.57 – 5.51 (*m*, 4 H), 4.15 (*bs*, 4 H), 3.86 – 3.52 (*m*, 16 H), 2.97 (*t*, *J* = 8 Hz, 4 H), 1.99 – 1.97 (*m*, 4 H), 1.91 – 1.87 (*m*, 4 H), 1.61 (*bs*, 12 H); HRMS Calcd protonated formula C<sub>55</sub>H<sub>67</sub>N<sub>12</sub>O<sub>14</sub>S<sub>2</sub> 1183.4341, found 1183.4399.

It is noted that the commercial ICG obtained from Sigma-Aldrich, as well as compound **3** prepared in our laboratory is a mixture of isomers as determined by high-performance liquid chromatography analysis. This mixture is undoubtedly a mixture of E/Z isomers of the polyene linker. No attempt was made to separate this mixture into the component stereoisomers,

and in all cases, the mixture was used for *in vivo* studies. To the best of our knowledge, such mixtures are used in all biological studies that involve ICG. This fact means that compound **9** is also a mixture of E/Z stereoisomers. It is structurally pure based on the connectivity shown for compound **9**, as indicated by <sup>1</sup>H NMR and high-resolution mass spectral analysis, however. This mixture of compound **9** was used for all *in vivo* studies, in accord with all previous work using ICG dyes.

### 3 Result

Figure 5 shows example fluorescence images obtained by FDOT with mice injected with 25 μM ICG (a), 25 μM ethanolamine-2-nitroimidazole-ICG (b), and 25 and 15 μM piperazine-2-nitroimidazole-ICG (c) and (d), obtained over 5- to 7-h period. Each image is 9 cm by 9 cm in *x* and *y* spatial dimensions at the corresponding target depth and the color bar represents the reconstructed dye concentration in μM. ICG was completely washed out after 3 h and the maximum fluorescence concentrations obtained from reconstructed images at 1, 15, 30, 60, 120, 180, and 300 min postinjection were 0.044, 0.066, 0.078, 0.033, 0.029, 0.025, and 0.000 μM, respectively, after subtraction of background value of 0.06 μM. However, for targeted conjugates, the maximum fluorescence concentrations measured postinjection of 25 μM ethanolamine-2-nitroimidazole-ICG were 0.028, 0.037, 0.041, 0.037, 0.036, 0.032, 0.026, and 0.025 μM above the background, and that of 25 μM piperazine-2-nitroimidazole-ICG postinjection were 0.064, 0.131, 0.111, 0.105, 0.072, 0.061, 0.044, and 0.044 μM above the background, obtained at 1, 15, 30, 60, 120, 180, 300, and 420 min. The improvement of the second-generation dye over the first is 2 to 3.5 times during the first 3 h postinjection period and 1.8 times after 3 h postinjection. The maximum fluorescence concentration with 15 μM piperazine-2-nitroimidazole-ICG postinjection was approximately 0.040 μM higher than the background shown in the figure. The ICG fluorescence intensity completely washed out after 3 h, while the targeted piperazine-2-nitroimidazole-ICG had a strong residue in the tumor after 7 h. Figure 6(a) through 6(d) shows the corresponding fluorescence images obtained from Odyssey Imaging system of the tumors injected with ICG (a), ethanolamine-2-nitroimidazole-ICG (b), and piperazine-2-nitroimidazole-ICG (c) and (d). The signal intensity with injection of 2-nitroimidazole-ICG conjugates, (b) through (d), is substantially higher than that of ICG (a), and the intensity of piperazine-2-nitroimidazole-ICG injection is substantially higher than that of ethanolamine-2-nitroimidazole-ICG. Two areas of higher and lower fluorescence intensity in each image obtained with the Odyssey system were selected for comparison to the corresponding tumor hypoxic areas in IHC images revealed with brown staining in 40× and 400× magnifications [middle column: lower hypoxic areas (e) through (l), right column: higher hypoxic areas (m) through (t)]. Note that the hypoxia conditions of these four excised tumor samples are statistically the same because the sizes of the tumors are similar.<sup>27</sup> However, the sensitivity or signal intensity of different dye conjugates at different concentrations is different and can be seen in these images. Within each image, the higher and lower signal intensity areas correspond to higher (more brown stains) and lower (less brown stains) hypoxic areas. To quantitatively compare the high- and low-signal-intensity areas within each image to hypoxia condition, four windows of size 1 × 1 mm in the high-signal-intensity areas and four windows of same size in the low-intensity areas are chosen and the computed percentage

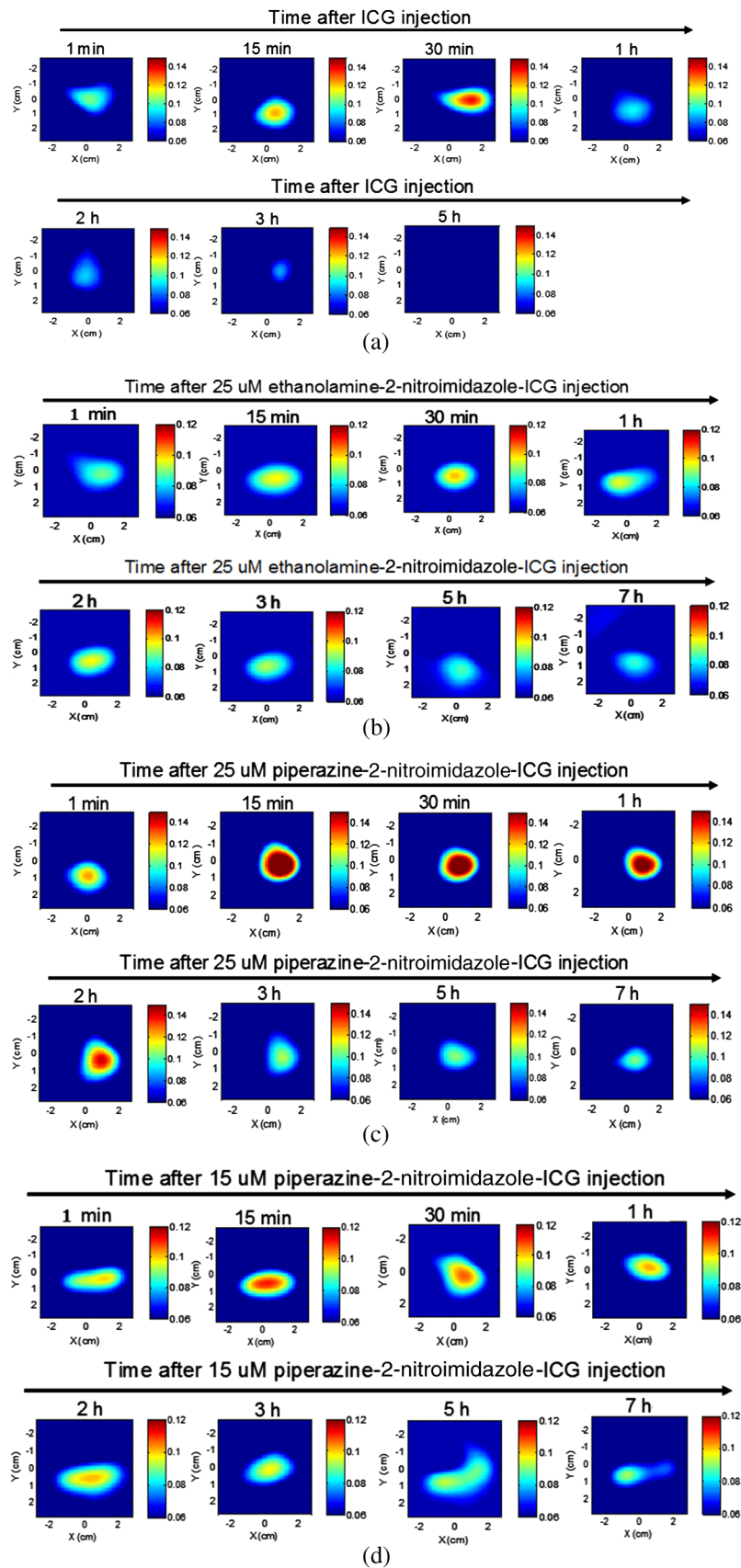


**Fig. 5** Fluorescence tomography images of four mice obtained over 5 to 7 h. (a) Images of mouse with tumor size of 10 mm injected with ICG and monitored over 5 h. (b) Images of mouse with tumor size of 8 mm injected with 25  $\mu$ M ethanolamine-2-nitroimidazole-ICG and monitored for 7 h. (c) Images of mouse with tumor size of 8 mm injected with 25  $\mu$ M piperazine-2-nitroimidazole-ICG and monitored for 7 h. (d) Images of mouse with tumor size of 8 mm injected with 15  $\mu$ M piperazine-2-nitroimidazole-ICG and monitored for 7 h. The time points are marked on images. The background value is 0.06  $\mu$ M in all images.

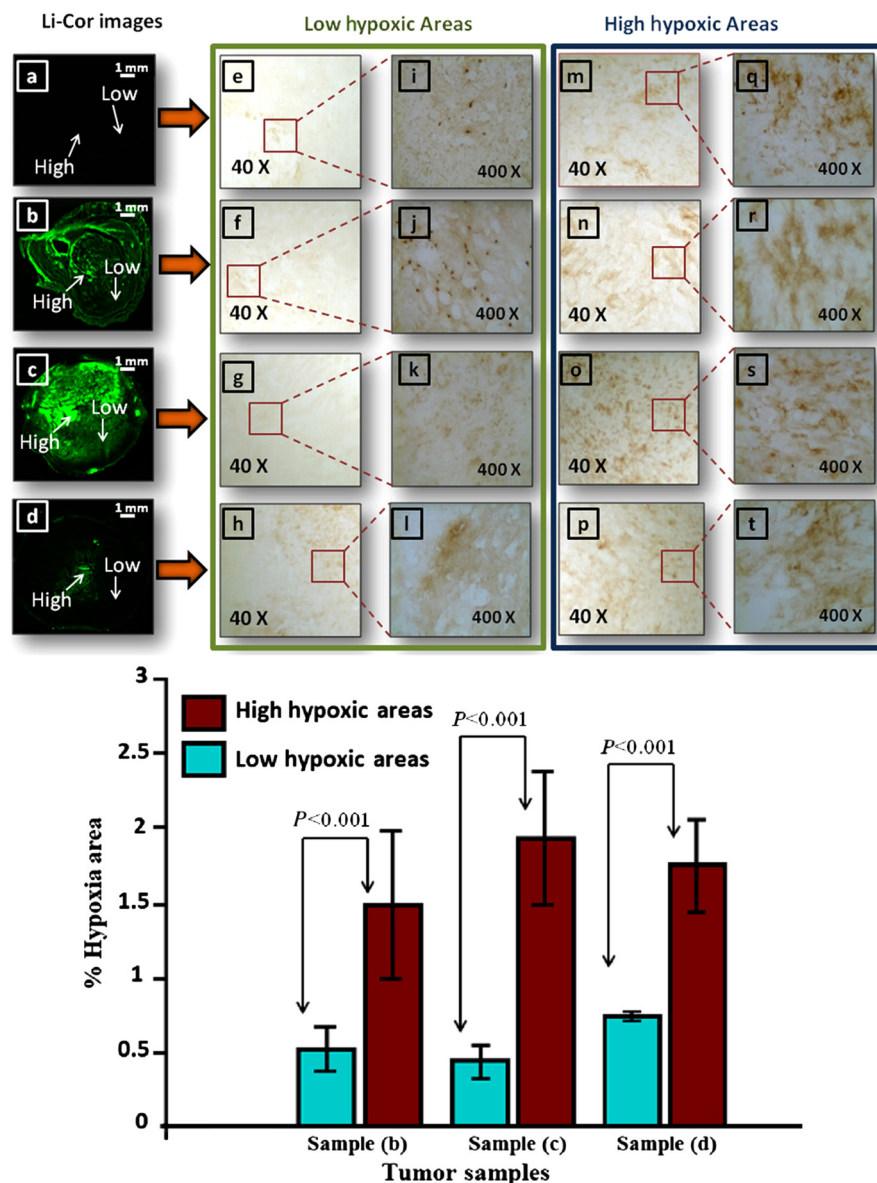


**Fig. 6** Top: The corresponding *ex vivo* fluorescence images acquired from the Odyssey Imaging system of (a) mouse image injected with 25  $\mu\text{M}$  ICG, (b) mouse image injected with 25  $\mu\text{M}$  ethanolamine-2-nitroimidazole-ICG, (c) and (d) corresponding images of two mice injected with 25 and 15  $\mu\text{M}$  piperazine-2-nitroimidazole-ICG, respectively, (e) through (h) corresponding IHC stains (40x, brown) at low tumor hypoxic area as marked at corresponding images, (m) through (p) corresponding IHC stains (40x) at higher hypoxic area, (i) through (l) corresponding IHC stains at low hypoxic area (400x, brown), and (q) through (t) corresponding stains at higher hypoxic area. Scale bar is 1 mm in images. Bottom: Percentage of hypoxic area from low fluorescence intensity area (green) and higher intensity area (red) of samples (b) through (d).

of hypoxic areas are shown in the bottom of Fig. 6. The high- and low-signal-intensity areas in each sample correlate with measured high and low hypoxic percentages. In the case of ICG, the signal intensity was too low and quantitatively comparison was not performed.

Figure 7 shows the comparison of average maximum fluorescence concentration of three groups of mice injected with ICG ( $n = 2$ ), ethanolamine-2-nitroimidazole-ICG ( $n = 2$ ), and piperazine-2-nitroimidazole-ICG ( $n = 3$ ) in 25  $\mu\text{M}$  concentration. The statistical significance was achieved between piperazine-2-nitroimidazole-ICG and ethanolamine-2-nitroimidazole-ICG, and piperazine-2-nitroimidazole-ICG and untargeted ICG beyond 60 min postinjection. The exponential fitting of the washout period of each dye is also shown in the figure. This figure demonstrates that the second-generation dye

conjugate had much higher fluorescence signal strength than that of the first-generation dye. On average, the ratios of fluorescence concentration of piperazine-2-nitroimidazole-ICG-injected tumors were 2.4 times higher within 3 h postinjection period than that of ethanolamine-2-nitroimidazole-ICG-injected tumors, and 1.7 times higher beyond 3 h postinjection. The kinetics of the two conjugates is also different. The fluorescence signal from piperazine-2-nitroimidazole-ICG quickly reached maximum at 15 min postinjection and then declined and remained flat with approximate half-life ( $t_{1/2}$ ) of 6 to 7 h, while the signal of ethanolamine-2-nitroimidazole-ICG reached maximum at 30 min postinjection and then slowly reduced and remained flat with approximate  $t_{1/2}$  of 9 to 10 h. The fluorescence signal of ICG reached maximum at 30 min postinjection and then quickly washed out with approximate  $t_{1/2}$  of 30 min.

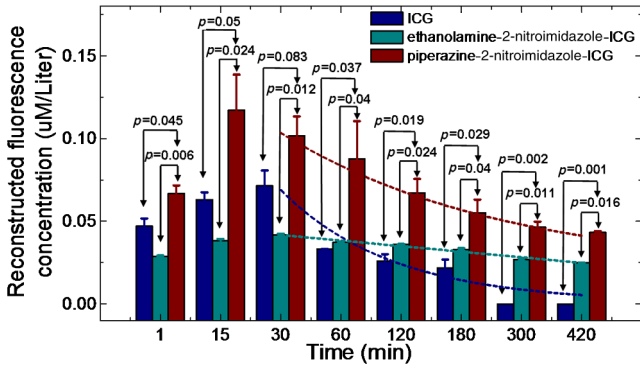


**Fig. 7** Comparison of reconstructed fluorescence concentration (maximum) versus time (min) of 25  $\mu\text{M}$  ICG, ethanolamine-2-nitroimidazole-ICG, and piperazine-2-nitroimidazole-ICG with tumor center located at 1.5 cm. The exponential fitting of the washout period of each dye is also shown.

For both targeted dye conjugates, the optimal window to assess tumor hypoxia is beyond 3 h postinjection, when free untargeted ICG is washed out completely.

We conducted another set of experiments with three sets of mice injected with ICG ( $n = 2$ ), first-generation conjugate ( $n = 2$ ), and second-generation conjugate ( $n = 2$ ) in 50  $\mu\text{M}$  concentration. On average, the ratios of fluorescence concentration of piperazine-2-nitroimidazole-ICG-injected tumors were 2.4 times higher within 3 h postinjection period than that of ethanolamine-2-nitroimidazole-ICG-injected tumors, and 1.6 times higher beyond 3 h postinjection. The measured kinetics of each dye conjugate is the same as reported above for 25  $\mu\text{M}$  injection.

One experiment was performed by imaging the piperazine-2-nitroimidazole-ICG-injected mouse 24 h later to evaluate how long the dye may remain in the tumor. Figure 8 shows the FDOT images obtained postinjection from 1 min to 24 h. The fluorescence signal strength after 3 h postinjection remains at similar levels. Although our observation is limited, this example does suggest that the piperazine-2-nitroimidazole-ICG may remain for a longer period of time in the tumor, which allows for *in vivo* targeting of tumor hypoxia.

To further evaluate the sensitivity of piperazine-2-nitroimidazole-ICG, we have conducted two sets of experiments with mice injected with 25 ( $n = 3$ ) and 15  $\mu\text{M}$  ( $n = 3$ ) concentrations and

tumors located at 1.5 and 2.0 cm depths, respectively. The average fluorescence signals and the standard deviations are shown in Fig. 9. For both concentrations at both depths, the targeted piperazine-2-nitroimidazole-ICG remains in tumor area beyond 3 h. At a deeper depth of 2 cm, both concentrations yield the same level of fluorescence signals beyond 3 h. Thus, the tumor depth did not affect tumor imaging.

To quantify the hypoxia conditions of two different groups of mice injected with ICG and dye conjugates, light microscopy (40 $\times$ ) images of the IHC samples were analyzed with Image *J* software. The mean hypoxia percentages for the piperazine-2-nitroimidazole-ICG, ethanolamine-2-nitroimidazole-ICG, and ICG groups were 2.29% ( $\pm 0.72$ ), 2.2% ( $\pm 0.54$ ), and 1.98% ( $\pm 0.30$ ), respectively. As expected, there is no statistical difference in tumor hypoxia conditions between the three groups, indicating the tumor model is consistent. However, the tumor size measured from the excised sample was found to strongly correlate with the percentage of hypoxia,<sup>27</sup> as shown in Fig. 10, for all tumor samples (Pearson correlation = 0.888,  $p < 0.001$ ). Similarly, the fluorescence images from the Odyssey system of the entire tumor sample were also analyzed by the Image *J* software. Figure 11 shows the mean fluorescence signals and standard deviations of the three sets of mice injected with ICG, first-

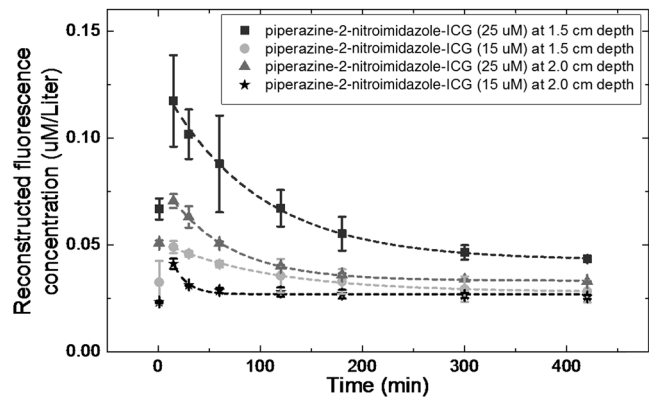


**Fig. 9** Average reconstructed fluorescence concentration (maximum) versus time (min) of piperazine-2-nitroimidazole-ICG injection at 25 and 15 M concentration with tumors located at depth of 1.5 cm (square and solid circle) and 2 cm (triangle and star).

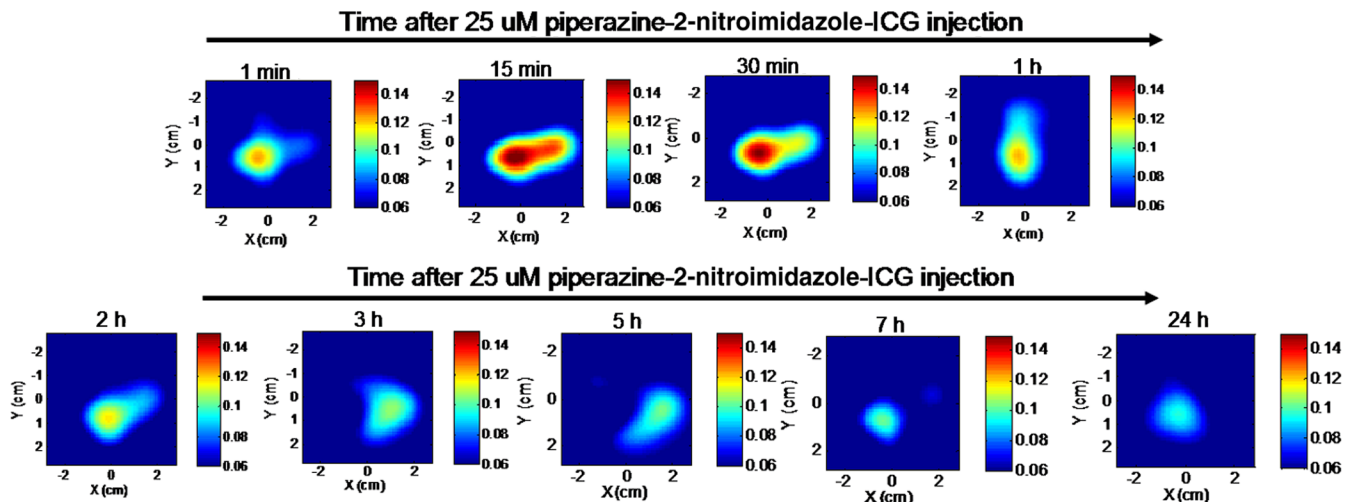


**Fig. 8** Fluorescence tomography images of one mouse obtained over 24 h. The mouse with tumor size of 10 mm injected with 25  $\mu\text{M}$  piperazine-2-nitroimidazole-ICG and monitored over 24 h. The time points are marked on images.

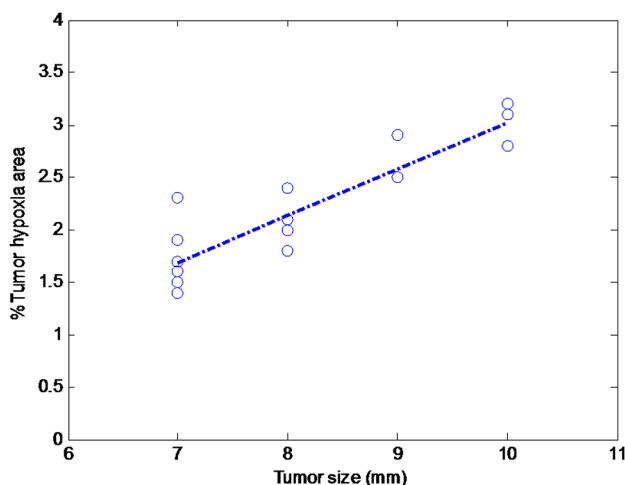


**Fig. 10** Correlation of measured tumor size versus percentage hypoxia area for all tumor samples ( $r = 0.888$ ,  $p < 0.001$ ).

and second-generation conjugates in 25 [Fig. 11(a)] and 50  $\mu\text{M}$  [Fig. 11(b)] concentrations. In Fig. 11(a), the mean signal strengths were 3.0 ( $\pm 0.98$ ), 21.7 ( $\pm 3.82$ ), and 37.7 ( $\pm 2.22$ ), respectively. The signal strength of second-generation dye over the first is 1.7 times, and the second- and first-generation dyes over ICG are 12.6 and 7.2 times. In Fig. 11(b), the mean fluorescence signals are 7.45 ( $\pm 0.91$ ), 29.6 ( $\pm 11.38$ ), and 48.6 ( $\pm 1.55$ ), respectively. On average, the fluorescence signal strength of second-generation dye over the first is 1.6 times, and second- and first-generation dyes over ICG are 6.5 and 4.0 times, respectively. These results from histological sections imaged with the Odyssey Imaging system scanner support the *in vivo* findings.

#### 4 Discussion and Summary

One method to improve tumor imaging is to improve the bioavailability<sup>31</sup> of the dye conjugate. A piperazine unit is common in many drugs,<sup>32</sup> so we incorporated a piperazine linker with the goal of increasing bioavailability<sup>33</sup> of the dye conjugate. We do not believe that the piperazine *per se* exhibits any influence

on the hypoxia targeting. However, if the bioavailability of the dye conjugate leads to a greater concentration in the tumor, presumably, enzymatic reduction of the nitro group will lead to an increased concentration of the dye conjugate. We believe that the observed greater distribution of piperazine-2-nitroimidazole-ICG in tissue may be due to the larger number of carbon atoms and slightly diminished polarity, which increases solubility in tissue when compared to the ethanolamine-2-nitroimidazole-ICG. Increased solubility would lead to a greater percentage of dye reaching the tumor, along with other tissues; however, selective hypoxia binding of the dye should lead to a larger percentage of dye conjugate in the tumor relative to other tissues, which would be measured as greater long-lasting fluorescence intensity. Indeed, we have observed increased fluorescence intensity of excised mouse tissues, such as liver and kidney, injected with piperazine ICG as compared with the tissues injected with ethanolamine-2-nitroimidazole-ICG, as well as enhanced tumor imaging.

2-nitroimidazole compounds are reduced in hypoxic cells and irreversibly bind to macromolecules (protein, nucleotides, etc). The bound compounds would remain until cell metabolism removed the macromolecules. It is well documented that the stability and half-life of the compound in the cells are dependent on cell type.<sup>34</sup> Different researchers have observed the turnover rates of hypoxic tumor cells with half-lives ranging from 17 to 49 h in various solid tumors. Due to animal study constraints, we did not image every mouse beyond 7 h, except for one. As shown in Fig. 8, the fluorescence image obtained at 24 h is about the same level as that obtained at 3 h, which suggests that the optimal window to image hypoxia condition of the tumor is at least between 3 to 24 h. Future studies will be focused on assessing oxygen-related treatment effects of tumor hypoxia using hypoxia dyes as indicators.

The extinction coefficient of ethanolamine-2-nitroimidazole-ICG reported in this work was slightly lower than that reported in our initial work<sup>19</sup> and the extinction coefficient of the ICG is the same as that reported before. Because the dye conjugates are difficult to make and the cost of 2-nitroimidazole is high, the amount of powder used for making fresh dyes used for each testing and animal experiment in this work is small

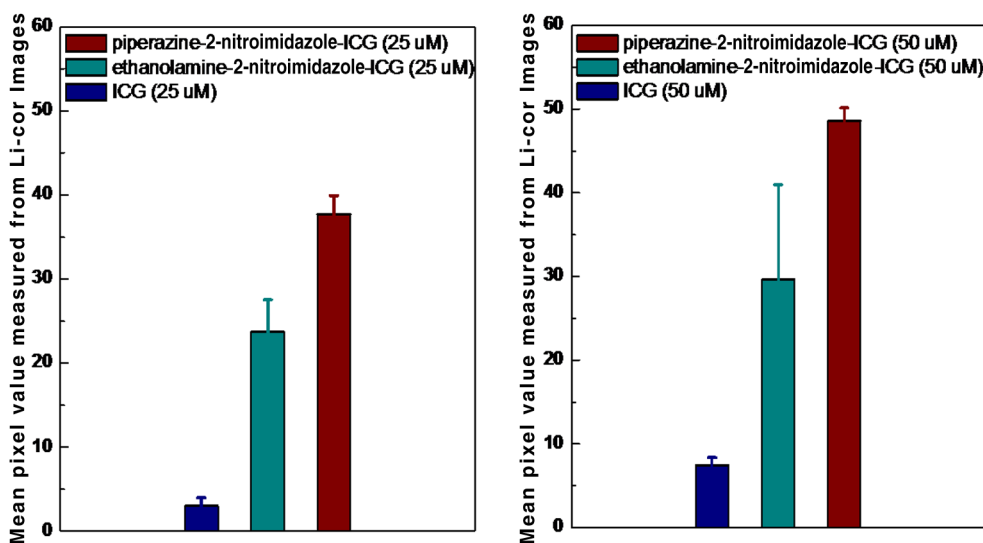


**Fig. 11** (a) The mean fluorescence signals and standard deviations of the three sets of mice injected with ICG, ethanolamine-2-nitroimidazole-ICG, and piperazine-2-nitroimidazole-ICG in 25  $\mu\text{M}$  concentrations. The mean signal strengths were 3.0 ( $\pm 0.98$ ), 21.7 ( $\pm 3.82$ ), and 37.7 ( $\pm 2.22$ ), respectively. (b) The mean fluorescence signals and standard deviations of the three sets of mice injected with ICG, ethanolamine-2-nitroimidazole-ICG, and piperazine-2-nitroimidazole-ICG in 50  $\mu\text{M}$  concentration. The mean fluorescence signals were 7.45 ( $\pm 0.91$ ), 29.6 ( $\pm 11.38$ ), and 48.6 ( $\pm 1.55$ ), respectively.

(0.3 to 0.7 mg) as compared with ICG (1.5 to 2 mg) and the scale precision may have affected the measurements. However, a similar amount of ethanolamine-2-nitroimidazole-ICG and piperazine-2-nitroimidazole-ICG were measured and thus the comparison of the extinction coefficients of two dyes should not be affected by the scale precision.

Note that our initial work used PBS as a medium, whereas the current study used a sucrose solution to solubilize the dye conjugates. The conjugates were soluble in PBS; however, over the course of one day, a partial precipitation of the dye from the PBS was observed. For this reason, we began using the dye conjugate in a sucrose solution and the dye is completely dissolved with no aggregation or partial precipitation observed at the concentration range we used for *in vivo* studies. The difference in medium may contribute to some differences in measured optical properties compared to our initial work. Additionally, in order to obtain more blue edges of the emission spectra, we have used 730 nm excitation wavelength to measure quantum yields of all dyes, while earlier study used 755 nm as the excitation.<sup>20</sup> The 730 nm excitation provides more accurate estimation of the area of each emission spectrum for quantum yield calculation while it compromises the emission signal strength.

To conclude, we have synthesized a second-generation tumor hypoxia targeted 2-nitroimidazole-ICG conjugate using piperazine linker and validated its performance through *in vivo* tumor targeting experiments in mice. On average, the reconstructed maximum fluorescence concentration of the tumors injected with the second-generation dye was twofold higher than that injected with the first-generation dye within 3 h postinjection period and 1.6 to 1.7 times higher beyond 3 h postinjection. Both dye conjugates have approximately 5 to 10 h half-life. This result suggests that the optimal time-window for evaluating tumor hypoxia is between 3 and 10 h postinjection.

### Acknowledgments

This project was supported by Connecticut Public Health under Contract No. 2011-0141 and partially supported by NIH R01EB002136 and Donaghue Medical Research Foundation. The authors thank Professor Kevin P. Claffey, Department of Cell Biology, University of Connecticut Health Center, Farmington, and David Serwanski, Department of Physiology and Neurobiology, University of Connecticut, for their consultations on hypoxia staining using immunohistochemistry technique.

### References

1. K. A. Krohn, J. M. Link, and R. P. Mason, "Molecular imaging of hypoxia," *J. Nucl. Med.* **49**(Suppl 2), 129S–148S (2008).
2. S. Kizaka-Kondoh and H. Konse-Nagasawa, "Significance of nitroimidazole compounds and hypoxia-inducible factor-1 for imaging tumor hypoxia," *Cancer Sci.* **100**(8), 1366–1373 (2009).
3. A. Nunn, K. Linder, and H. W. Strauss, "Nitroimidazoles and imaging hypoxia," *Eur. J. Nucl. Med.* **22**(3), 265–280 (1995).
4. R. J. Hodgkiss, "Use of 2-nitroimidazoles as bioreductive markers for tumour hypoxia," *Anticancer Drug Des.* **13**(6), 687–702 (1998).
5. Z. Li and T. Chu, "Recent advances on radionuclide labeled hypoxia-imaging agents," *Curr. Pharm. Des.* **18**(8), 1084–1097 (2012).
6. L. B. Tran et al., "Hypoxia imaging with the nitroimidazole (18)F-FAZA PET tracer: a comparison with OxyLite, EPR oximetry and (19)F-MRI relaxometry," *Radiother. Oncol.* **105**(1), 29–35 (2012).
7. V. Ntziachristos, "Going deeper than microscopy: the optical imaging frontier in biology," *Nat. Methods* **7**(8), 603–614 (2010).
8. E. M. Sevick-Muraca, "Translation of near-infrared fluorescence imaging technologies: emerging clinical applications," *Annu. Rev. Med.* **63**, 217–231 (2012).

9. V. Ntziachristos, C. Bremer, and R. Weissleder, "Fluorescence imaging with near-infrared light: new technological advances that enable *in vivo* molecular imaging," *Eur. Radiol.* **13**(1), 195–208 (2003).
10. K. M. Tichauer et al., "Computed tomography-guided time-domain diffuse fluorescence tomography in small animals for localization of cancer biomarkers," *J. Vis. Exp.* (65) (2012).
11. S. B. Raymond et al., "Smart optical probes for near-infrared fluorescence imaging of Alzheimer's disease pathology," *Eur. J. Nucl. Med. Mol. Imag.* **35**(Suppl 1), S93–98 (2008).
12. V. A. Lawson et al., "Near-infrared fluorescence imaging of apoptotic neuronal cell death in a live animal model of prion disease," *ACS Chem. Neurosci.* **1**(11), 720–727 (2010).
13. L. Zhu et al., "In vivo optical imaging of membrane-type matrix metalloproteinase (MT-MMP) activity," *Mol. Pharm.* **8**(6), 2331–2338 (2011).
14. S. Oliveira et al., "Rapid visualization of human tumor xenografts through optical imaging with a near-infrared fluorescent anti-epidermal growth factor receptor nanobody," *Mol. Imag.* **11**(1), 33–46 (2012).
15. S. Kaur et al., "Recent trends in antibody-based oncologic imaging," *Cancer Lett.* **315**(2), 97–111 (2012).
16. N. C. Biswal et al., "Fluorescence imaging of vascular endothelial growth factor in tumors for mice embedded in a turbid medium," *J. Biomed. Opt.* **15**(1), 016012 (2010).
17. M. B. Aldrich et al., "Concentration of indocyanine green does not significantly influence lymphatic function as assessed by near-infrared imaging," *Lymphat. Res. Biol.* **10**(1), 20–24 (2012).
18. A. Corlu et al., "Three-dimensional *in vivo* fluorescence diffuse optical tomography of breast cancer in humans," *Opt. Express* **15**(11), 6696–6716 (2007).
19. C. Pavlik et al., "Synthesis and fluorescent characteristics of imidazole-indocyanine green conjugates," *Dyes and Pigments* **89**(1), 9–15 (2011).
20. N. Biswal et al., "Imaging tumor hypoxia by near-infrared fluorescence tomography," *J. Biomed. Opt.* **16**(6), 1–8 (2011).
21. G. Barker, P. O'Brien, and K. R. Campos, "Diamine-free lithiation-trapping of N-Boc heterocycles using *s*-BuLi in THF," *Org. Lett.* **12**(18), 4176–4179 (2010).
22. Y. Imaeda et al., "Discovery of imidazo[1,5-*c*]imidazol-3-ones: weakly basic, orally active factor Xa inhibitors," *J. Med. Chem.* **51**(12), 3422–3436 (2008).
23. Z. Wang et al., "[beta]-Lactone probes identify a papain-like peptide ligase in *Arabidopsis thaliana*," *Nat. Chem. Biol.* **4**(9), 557–563 (2008).
24. J. B. Birks, "Fluorescence quantum yield measurements," in *Standardization in Spectrophotometry and Luminescence Measurements: Proceedings of a Workshop Seminar Held at the National Bureau of Standards, Gaithersburg, Maryland, November, November 19-20, 1975*, US Department of Commerce, National Bureau of Standards (1976).
25. A. T. R. Williams, S. A. Winfield, and J. N. Miller, "Relative fluorescence quantum yields using a computer-controlled luminescence spectrometer," *Analyst* **108**(1290), 1067–1071 (1983).
26. S. A. Soper and Q. L. Mattingly, "Steady-state and picosecond laser fluorescence studies of nonradiative pathways in tricyanocyanine dyes—Implications to the design of near-IR fluorochromes with high fluorescence efficiencies," *J. Am. Chem. Soc.* **116**(9), 3744–3752 (1994).
27. E. M. Hendriksen et al., "Angiogenesis, hypoxia and VEGF expression during tumour growth in a human xenograft tumour model," *Microvas. Res.* **77**(2), 96–103 (2009).
28. V. Ntziachristos and R. Weissleder, "Experimental three-dimensional fluorescence reconstruction of diffuse media by use of a normalized Born approximation," *Opt. Lett.* **26**(12), 893–895 (2001).
29. A. Soubret, J. Ripoll, and V. Ntziachristos, "Accuracy of fluorescent tomography in the presence of heterogeneities: study of the normalized Born ratio," *IEEE Trans. Med. Imag.* **24**(10), 1377–1386 (2005).
30. <http://rsbweb.nih.gov/ij/index.html>.
31. V. H. Thomas et al., "The road map to oral bioavailability: an industrial perspective," *Expert Opin. Drug. Metab. Toxicol.* **2**(4), 591–608 (2006).
32. M. J. Neil, A. Smith, and P. Heckelman, *The Merck Index*, 14th ed., John Wiley and Sons, New Jersey (2006).
33. C. B. Vu et al., "Piperazine derivatives of [1,2,4]triazolo[1,5-*a*][1,3,5]triazine as potent and selective adenosine A2a receptor antagonists," *J. Med. Chem.* **47**(17), 4291–4299 (2004).
34. A. S. Ljungkvist et al., "Hypoxic cell turnover in different solid tumor lines," *Int. J. Rad. Oncol. Biol. Phys.* **62**(4), 1157–1168 (2005).